Curvilinear variable stiffness 3D printing technology for improved open-hole tensile strength

Sadben Khan[1], Kazem Fayazbakhsh[1]*, Zouheir Fawaz[1], Mahdi Arian Nik[2]

[1]Aerospace Engineering Department, Ryerson University, 350 Victoria Street, Toronto, ON, Canada M5B 2K3
[2]Department of Mechanical Engineering, McGill University, Macdonald Engineering Building, 817 Sherbrooke West, Montreal, QC, Canada H3A 2K6
**Corresponding author: kazem@ryerson.ca; Tel: (+1) 416-979-5000 ext. 6414; fax: (+1) 416-979-5056*

Abstract

Fused Filament Fabrication (FFF), one of the most popular processes of 3D printing, offers flexibility in manufacturing and introduces anisotropic properties to the final parts. With the use of Curvilinear Variable Stiffness (CVS) 3D printing technology, mechanical properties of the manufactured products can be further improved and optimized. In this work, we demonstrate how CVS design can improve open-hole tensile strength and failure strain of the manufactured specimens per ASTM D5766. In addition, the ratio of the specimen width to the hole diameter is considered as a design parameter and investigated. It is found that CVS design improves the failure strength by 38.0% for a larger hole diameter configuration (from 48.0 MPa to 66.2 MPa), while the improvement in failure strain (from 0.0125 mm/mm to 0.0130 mm/mm) is limited to only 4.0%. On the other hand, for a smaller hole diameter case, a substantial improvement of 52.5% in failure strain is obtained with the use of CVS design (from 0.0141 mm/mm to 0.0215 mm/mm), while 16.7% improvement in failure stress (76.0 MPa to 88.6 MPa) is less pronounced.

Keywords:

Curvilinear Variable Stiffness (CVS) design, Fused Filament Fabrication (FFF), 3D printing, Open-hole tensile strength

Additive Manufacturing Journal

https://doi.org/10.1016/j.addma.2018.10.013

1. Introduction

Increasingly, industry is using Additive Manufacturing (AM) techniques, or 3D printing, for lightweight and high performance products fabrication. The process of AM creates a 3D part layer by layer, as opposed to traditional subtractive manufacturing methodologies, where a part is made by removing the material. There have been significant advancements in 3D printing, especially Fused Filament Fabrication (FFF), over the past few years. In the FFF process, a filament is continuously fed into an extrusion head or nozzle. The material is heated to a molten state before it reaches the nozzle, where it can be deposited onto the platform [1]. Standard materials for filaments in FFF process are thermoplastics, like PolyLactic Acid (PLA), Acrylonitrile Butadiene Styrene (ABS), PolyCarbonate (PC), and polyamides. Although 3D printed components out of thermoplastics are ideal for prototyping due to their low cost and high dimensional accuracy, their low mechanical properties prevent their wide use in final engineering products. A significant amount of research has been done to improve mechanical performance of FFF 3D printed parts by reinforcing pure thermoplastics using short fibers [1-4] or continuous fibers [5-7].

Aside from filament materials, there are several manufacturing process and design parameters that impact mechanical performance of 3D printed parts. The parameters include: nozzle temperature, bed temperature, fan speed, printing speed, build orientation, layer thickness, raster angle, and infill percentage. Many researchers have studied the impact of raster angle on structural performance of 3D printed specimens, e.g. tensile strength and modulus. Carneiro et al. [8] compared raster angles of 0°, 45°, 90°, 0-90°, and ±45° using specimens manufactured per DIN 53504 standard with an infill of 100%. It has been shown that 0° orientation set of samples had the highest tensile strength and modulus, while the ±45 ones showed the lowest. Hossain et al. [9] investigated three build orientations each with three different raster angles: 0°/90°, 30°/-60°, and 45°/-45°. For XYZ build orientation, it was observed that 0°/90° specimen had the highest tensile strength and modulus. Zaldivar et al. [10] manufactured specimens per ASTM D638 with three different build orientations and raster angles with a layer thickness of 0.254 mm. It has been found that for XYZ build orientation, 0° raster angle gives a tensile strength of 55.8 MPa and a modulus of 2.28 GPa, which was higher than properties achieved by samples made by 45° and 90° raster angles. Ziemian et al. [11] used a dogbone-shaped specimen made of ABS-P400 to investigated tensile strength and modulus of four different raster angles: 0°, 45°, 90°, and +45°/-45° . The ultimate and yield strength, and effective modulus were the highest for 0° specimens followed by +45°/-45°, 45°, and 90° specimens. A similar trend was reported by Lanzotti et al. [12]. Hill and Haghi [13] changed raster angles between 0° and 90° in 15° increments and manufactured six specimens for each raster angle, a total of 42 tensile samples. The highest tensile strength of 59.8 MPa was observed for 0° raster angle, while the lowest value of 18.0 MPa was found for 75° raster angle. In the above research works, it is shown that the angle of straight rasters, which is constant within each layer, has a substantial impact on mechanical properties of 3D printed parts.

The significance of using a curvilinear variable stiffness design to improve structural performance of final parts was first demonstrated in the field of fiber reinforced composites. Yau and Chou [14] created curvilinear fibers around a hole by inserting metal pins into woven fabrics

prior to curing, thereby resulting in improved open-hole strength. Hyer and Charette [15] designed a laminate with fibers aligned along the principal stress direction and improved the tensile loading of a plate with a central hole. The tensile load of the laminates with curvilinear fibers calculated by FEM was shown to be increased up to 60% compared to a quasi-isotropic laminate. They also found that none of the optimized variable stiffness laminates have a buckling load as high as the quasi-isotropic laminate. In another study, Hyer and Lee [16] showed that one could improve the buckling load of a plate with a circular hole using a curvilinear fiber path. They considered a quarter of the plate and divided it into 18 regions with a single fiber orientation through the thickness of the laminate. A gradient-based technique was then used to determine the optimum fiber orientation within each region. They obtained discrete distribution of fiber orientations that could improve the buckling load of the composite plate up to 85% over the quasi-isotropic laminate. It was found that the curvilinear fibers transfer the load from the plate center toward the edges, which are supported, thus increasing the buckling load. To reduce the computational cost of the optimization problem solved by Hyer and Lee [16], Huang and Haftka [17] considered a symmetric six-layer $[(C\text{-}0)/\pm45]_s$ and $[C\text{-}0]_6$ plates with a central hole. The C-0 represents a layer that is divided into a small near field around the hole, where the fiber orientation could vary discretely, and a large far field region away from the hole, where the fiber orientation is fixed at 0°. It was shown that optimizing the fiber orientation in the near field region could improve the load carrying capacity of the $[C\text{-}0]_6$ plate by over 100%, while the improvement for the $[(C\text{-}0)/\pm45]_s$ plate was 88%. That being said, they suggested the $[(C\text{-}0)/\pm45]_s$ design might be preferred because of the robustness offered by ±45 plies under off-design conditions. Other researchers, for example Banichuk [18, 19], Pedersen [20, 21], and Duvaut et al. [22] also focused on finding the optimum discrete fiber angle distribution within a laminate to improve the buckling load and strength of the laminate, where the manufacturing issues were not a concern. In another study, Tosh and Kelly [23] proposed to align the fibers with the principal stress vectors and load paths to increase the plate strength. They used a dry tow steered onto a tacky resin film to manufacture the fiber paths with small radii. The tensile tests on the manufactured specimens showed that the specific strength improved by up to 62% and 85%, respectively, for an open hole and pin-loaded configuration. Using a similar approach, Li et al. [24-26] increased the peak load of a bolted joint in composite specimens up to 169% and its bearing strength up to 36% compared to a quasi-isotropic design. Although the above studies require a prohibitive computational cost for the optimization process and did not design for manufacturing, they are promising since they demonstrate the potential of optimizing the fiber angle distribution within the laminate for improving the performance of a composite laminate.

Unlike fiber reinforced composite designs described above, load-oriented design concept is not well established for FFF 3D printing and currently designers mostly use straight rasters within each layer. Tam and Mueller [27] identified orienting material deposition along 3D principal stress vectors as the candidate for maximizing the strength-to-weight ratio for structural prints. They used Stress Line Additive Manufacturing (SLAM) to investigate two cases: planar geometries (SLAM Planar) using a commercial FFF platform; and Robot-Enabled SLAM for 2.5D cases. SLAM planar case demonstrated 1.6 times increase in yield load-to-weight ratio compared to straight rasters case. Robot-Enabled SLAM cases also showed a 25% improvement in stiffness, and a 76% and 27% improvement in ultimate strength capacity and ductility after

initial failure, respectively. Although numerical and experimental results showed the benefit of material redistribution by stress lines, they are not statically conclusive since the number of tests conducted is not sufficient. Furthermore, Tam and Mueller [27] showed the improvement for a complex and unconventional design and did not follow a standard test method regarding specimen geometry and dimensions, and testing procedure to characterize mechanical properties of SLAM cases.

In this research paper, to properly characterize mechanical properties of 3D printed parts, ASTM D5766 standard test method is followed to demonstrate that open-hole tensile strength can be improved using Curvilinear Variable Stiffness (CVS) 3D printing technology. In the following sections, first, specimen geometry, configuration, and testing procedure are described per ASTM D5766. Then, an analytical approach is described to find load paths using the analogy of field equations for potential flow around a cylinder. A MATLAB subroutine is developed to convert the load paths to GCODE for 3D printing. Next, experimental testing is performed and tensile strength for different specimen configurations is obtained. Finally, a discussion of the performance of CVS 3D printed specimens is presented before the closing remarks and recommendations for future research.

2. Specimens design and manufacturing

Specimen geometry, stacking sequence, and testing procedure are designed per ASTM D5766. Then, an analytical approach is described for obtaining the load paths for improving open-hole tensile strength of the specimens.

2.1. Specimens geometry and stacking sequence

A specimen with a centrally located hole according to the configuration B per ASTM D5766 is selected in this research for open-hole tensile strength testing. The width, length, and thickness of the specimen are 36mm, 150mm, and 2.24 mm, respectively with a specimen grip length of 35 mm. The notch consists of a hole centrally located by length and width of the specimen. Figure 1 shows the schematic drawing of open-hole tension test specimen.

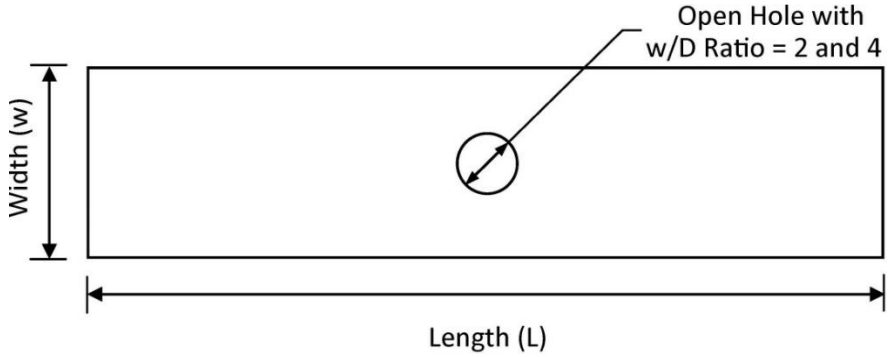

Figure 1. Schematic drawing of open-hole tension test specimen.

Experimental testing is extended to investigate the influence of the specimen width to the hole diameter (w/D). Therefore, two cases with w/D of 2 (hole diameter of 18 mm) and 4 (hole diameter of 9 mm) are designed and manufactured. The standard laminate is balanced and

symmetric, and has multi-directional fiber orientations. To demonstrate improvements in load carrying capacity that can be achieved using CVS design, an optimum constant stiffness design is considered as the baseline with filaments aligned along with the loading direction (0°). Previous study [17] suggested including ±45° layers can improve design robustness under off-design conditions. As a result, a $[\pm 45/0_6]_s$ stacking sequence is considered as the baseline, which has 16 layers, each 0.14 mm in thickness. For CVS design, 0° layers are replaced with optimum load paths resulting in a $[\pm 45/(CVS)_6]_s$ stacking sequence, where CVS denotes Curvilinear Variable Stiffness layers. According to ASTM D5766, five specimens per test conditions are designed, manufactured, and tested. Figure 2 illustrates the stacking sequence notation used in this research paper.

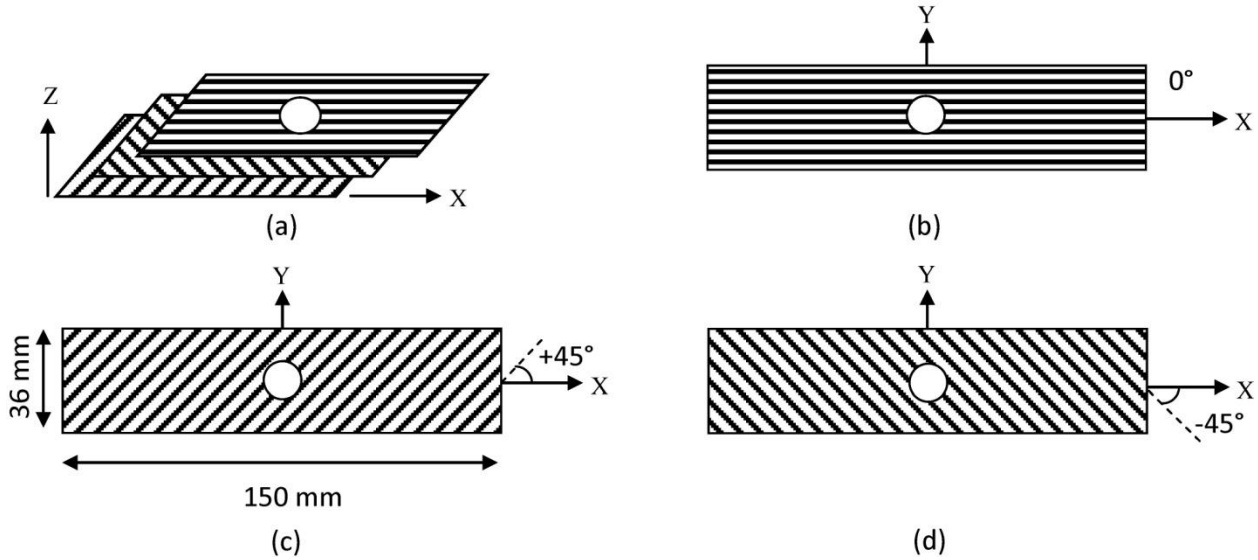

Figure 2. Stacking sequence illustration: (a) +45°, -45°, and 0° layers stacked on top of each other along the z-axis resulting in [±45/0] notation; (b) 0° layer; (c) 45° layer; and (d) -45° layer.

Hole diameter (D) and specimen thickness are measured using a dial caliper and reported to the nearest 0.025 mm (0.001 in). A micrometer is used to measure the specimen width, which is also reported to the nearest 0.025 mm (0.001 in). Since strain response local to the hole is of interest, one extensometer to the specimen edge is attached and it is ensured that the hole is located within the extensometer gage section. A testing speed of 2 mm/min is chosen to give rupture within 0.5 to 5-min testing time and force versus strain is recorded with a target minimum of 100 data points.

2.2. Coupons load paths

An analogy to stress trajectories in the case of open hole tension can be taken from fluid flow around a cylinder. Such an analogy can be helpful as fluids tend to flow over a surface smoothly in one continuous streamline to take the path of least resistance. To improve stress concentrations, such a property of fluid flow would be useful in curving the fiber path around the hole with slow transitions and continuous fibers [28].

To model these load paths to be used in 3D printing, the field equations for potential flow were considered as the trajectories of a distance r from the reference point. The analytical solution for the potential flow around a cylinder allows determining the load paths at specific distances from center of the hole that were proportional to the width of the extrudate.

The velocity potential can be obtained by the analytical solution to the unit flow around a cylinder:

$$\phi(r,\theta) = r\left(1 + \frac{R^2}{r^2}\right)\cos\theta \tag{1}$$

Where, r is the distance from the hole center, θ is the angle from the x-axis, and R represents the hole radius [29].

The partial derivatives of the potential function (Eq. 1) can be written as:

$$V_r = \frac{\partial\phi}{\partial r} = \left(1 - \frac{R^2}{r^2}\right)\cos\theta \tag{2}$$

$$V_\theta = \frac{1}{r}\frac{\partial\phi}{\partial\theta} = -\left(1 + \frac{R^2}{r^2}\right)\sin\theta \tag{3}$$

Where V_r is the radial component and V_θ denotes the tangential component in the polar reference frame.

The superposition of three potentials were taken with respect to the origin, with the spacing between them being the width of the specimen. The superposition principle allowed for the creation of a boundary at the edge of the specimen, by creating essentially what are “virtual” holes outside the coupon boundary. The corresponding mirrored vortexes would eliminate each other’s influence, thereby generating only a u component at the boundary. Adding the super position is necessary, as without the cancellation, the load paths would exit the coupon boundary.

The velocity components were then calculated across a mesh that represented the boundaries of the test specimen described in Section 2.1. The velocity components in the polar reference frame were then translated to the Cartesian reference frame to calculate the trajectories. Figure 3 shows the trajectories with the load paths overlaid to illustrate how the velocity components calculated at each point in the mesh are interpolated into the load paths.

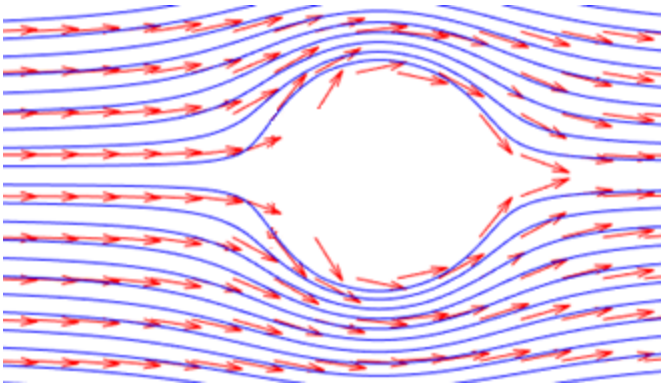

Figure 3. Trajectories with load paths overlaid.

Each streamline was considered as the centerline of a extrudate, with the spacing set as the extrudate width. Besides generating the material deposition trajectories, various coefficients are determined to account for the manufacturing parameters like the amount of filament deposited per distance traveled, extrudate thickness, and height. Many of these coefficients were determined with respect to the default settings of the Prusa i3 M2 printer.

As shown in Figure 4a, imposing the same spacing between the load trajectories caused them to converge around the hole indicating the stress concentration induced by the hole. In manufacturing of the CVS layer, a no-overlap strategy is used to avoid a thickness buildup. As a result, the extrudates around the hole just touch, whereas there are gaps between the extrudates in regions far from the hole. For ±45° raster layers, there is no gap and/or overlap between subsequent extrudates (100% infill) and they break when reaching the hole as opposed to curvilinear paths. The generated streamlines in MATLAB for the specimen with w/D=4 can be seen in Figure 4.

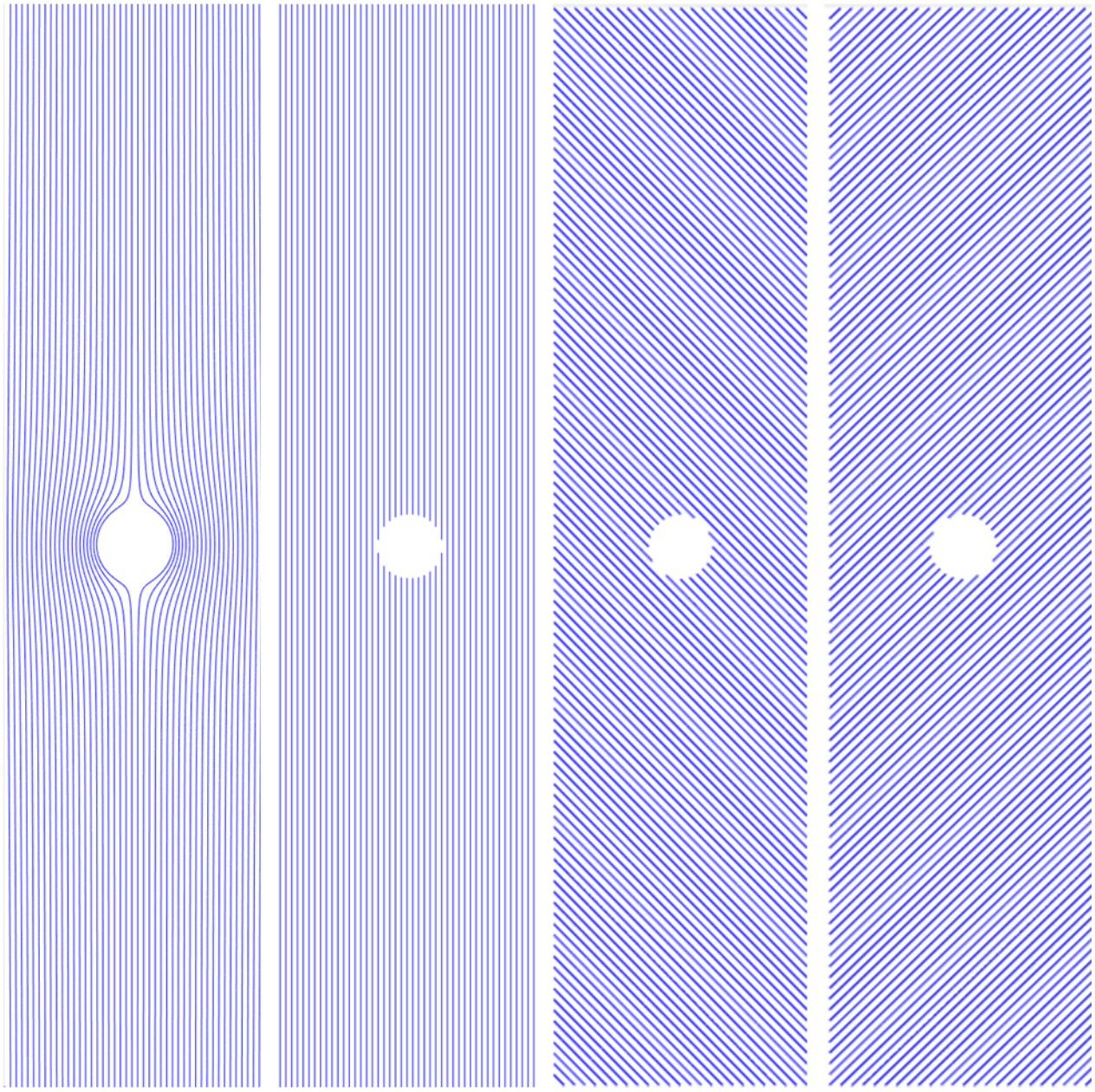

(a) (b) (c) (d)

Figure 4. The load paths for open-hole tensile specimen with w/D=4: (a) CVS, (b) 0°, (c) -45°, and (d) +45°.

2.3. Specimens manufacturing

For CVS designs obtained in Section 2.2, there is no commercially available tool to implement the infills. Therefore, a subroutine in MATLAB is developed to generate GCODE from those trajectories. As an example, the tool paths generated by this subroutine for printing the CVS layer for w/D=4 is visualized in Figure 5 using a commercial GCODE viewer, NCVIEWER. The material deposition always starts from the left side of a sample and finishes at

the right side. When the tool head (the nozzle) finishes placing one extrudate and reaches the right side, it returns to the left side along a 0° path without extruding any material. Figure 5a shows the tool paths with and without material deposition, and that is why 0° tool paths can be observed along with the curvilinear ones, while some of the 0° tool paths pass through the hole area. The diagonal stitch is the tool path from its initial location to the sample boundary and then to its final location after successfully printing the CVS layer. The tool paths with material deposition can be seen in Figure 5b and can be compared with the printed CVS layer (Figure 7).

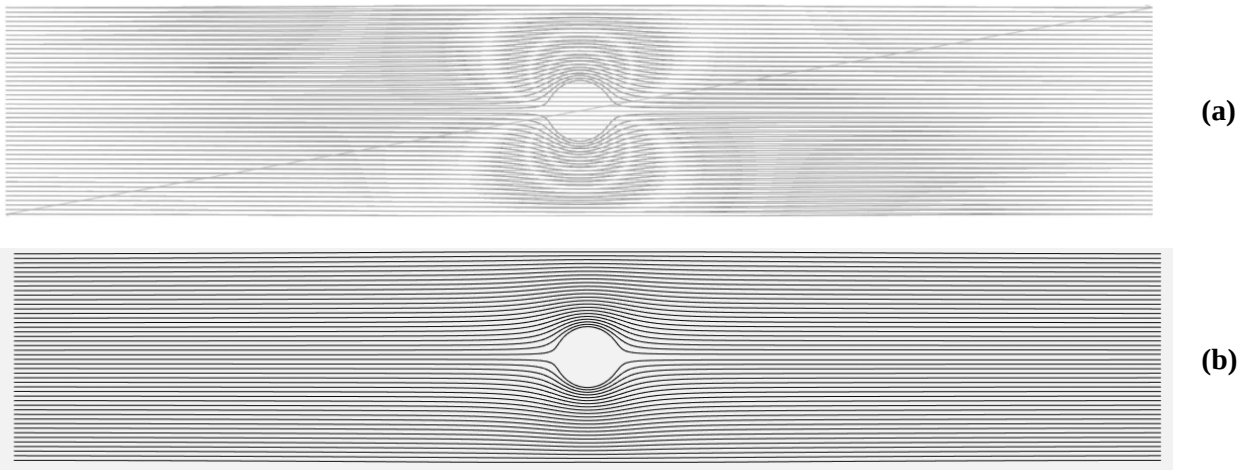

(a)

(b)

Figure 5. Tool paths for the CVS layer for w/D =4 in GCODE: (a) with and without material deposition; (b) with material deposition only.

Five sets of specimens are manufactured using Prusa i3 MK2S for each configuration described in Section 2.1. The manufacturing process and design parameters are given in Table 1.

Table 1. Manufacturing process and design parameters for specimens 3D printing.

Manufacturing/design Parameter	Value	Manufacturing/design Parameter	Value
Print direction	XYZ	Material	PLA
Filament diameter	1.75 mm	Nozzle diameter	0.4 mm
Layer height	0.14 mm	Nozzle temperature	215 °C
Bed temperature	60	Cooling	No fan cooling
Printing speed	2400 mm/min	Infill %	100% for ±45° layers

As mentioned in Section 2.2, for CVS layers, the extrudates around the hole just touch, whereas there are gaps between the extrudates in regions far from the hole. 0° layer has the same extrudates spacing as CVS far from the hole, while there is no gap and/or overlap between subsequent extrudates for ±45° layers (100% infill). As a result, 100% infill is used for ±45° layers, while the infill percentage for the CVS and 0° layers is governed by the design. Figure 6 shows placing of the extrudates along curvilinear paths during the manufacturing process and the completed layer is shown in Figure 7.

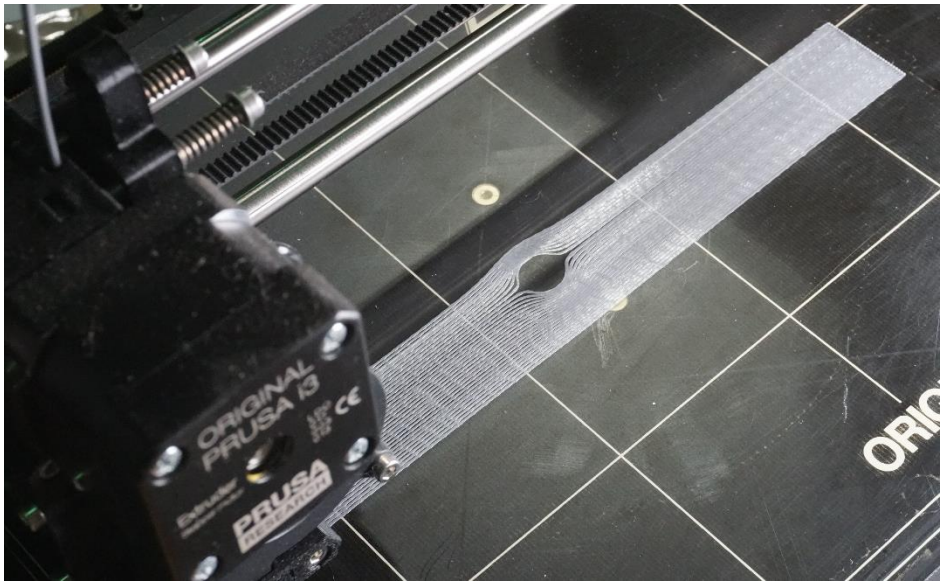

Figure 6. CVS layer during printing

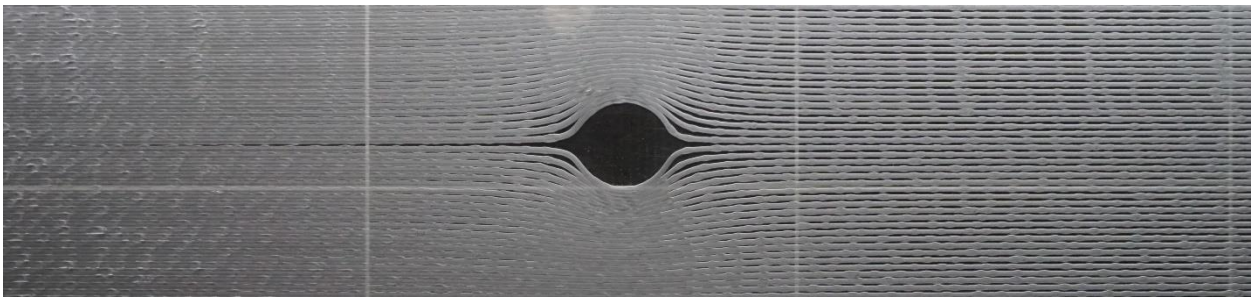

Figure 7. Completed CVS layer for w/D=4.

In addition, five sets of specimens with only straight rasters are manufactured using the same manufacturing process and design parameters explained above. Figure 8 shows a Variable Stiffness (VS) and Constant Stiffness (CS) specimen after 3D printing.

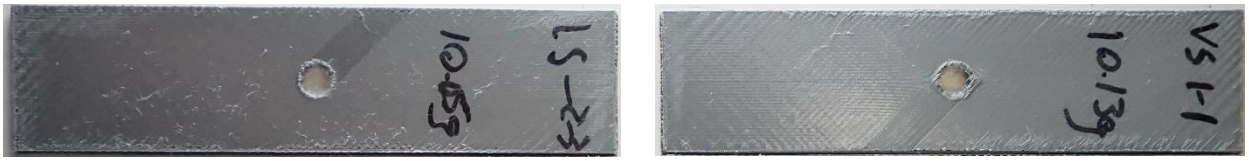

(a) **(b)**

Figure 8. Open-hole tensile specimens with w/D=4: (a) CS specimen; and (b) VS specimen.

The completed specimens were close in weight variation with the VS specimens weighing slightly less than the CS ones. The same process is followed and 5 sets of VS and CS specimens are manufactured for the other configuration, w/D=2. Table 2 shows the average weight and standard deviation for the manufactured specimens.

Table 2. Weight variation of manufactured VS and CS specimens

w/D ratio	Design	Stacking sequence	Average Weight (g)	Standard Deviation (g)
2	CS	$[\pm 45/0_6]_s$	9.57	0.11
	VS	$[\pm 45/(CVS)_6]_s$	9.24	0.14
4	CS	$[\pm 45/0_6]_s$	10.06	0.03
	VS	$[\pm 45/(CVS)_6]_s$	10.14	0.05

All manufactured specimens are tested using a United testing machine with a 10 kN load cell and the results are presented in Section 3. Figure 9 shows the test set-up including a VS specimen for w/D=4 inside the fixture with the extensometer.

Figure 9. The test set-up including a variable stiffness specimen (w/D=4), the fixture, and the extensometer.

3. Results and discussion

A constant crosshead speed of 2 mm/min is applied to the specimens until failure, while force versus strain is recorded. According to ASTM D5766, failures that occur at the hole are acceptable failure modes and are limited to Gage Middle (*GM), where they can be either Lateral (L), Angled (A), or Multi-mode (M), resulting in failure mode codes of LGM, AGM, and MGM. Ultimate open-hole tensile strength is calculated based on the gross cross-sectional area, ignoring the presence of the hole. All specimens for the two configurations (w/D=2 and 4) showed acceptable failure modes per the standard ranging from LGM and AGM to MGM. Figure 10 shows a VS specimen for w/D=4, where failure passes through the hole in the test specimen (LGM mode).

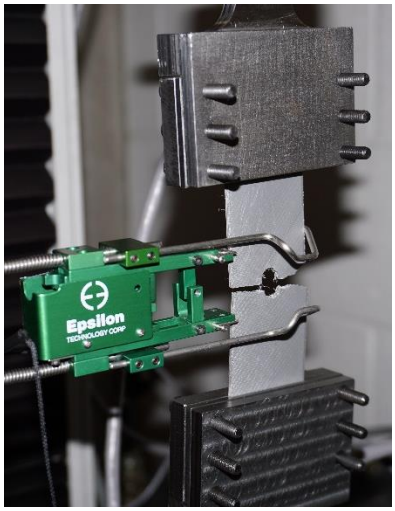

Figure 10. A VS specimen (w/D=4) after failure (LGM mode).

The stress-strain graph for a CS and a VS specimen with w/D=2 can be seen in Figure 11. It is evident that the use of CVS design significantly improves the failure strength for w/D=2 configuration, while the improvement in failure strain is limited.

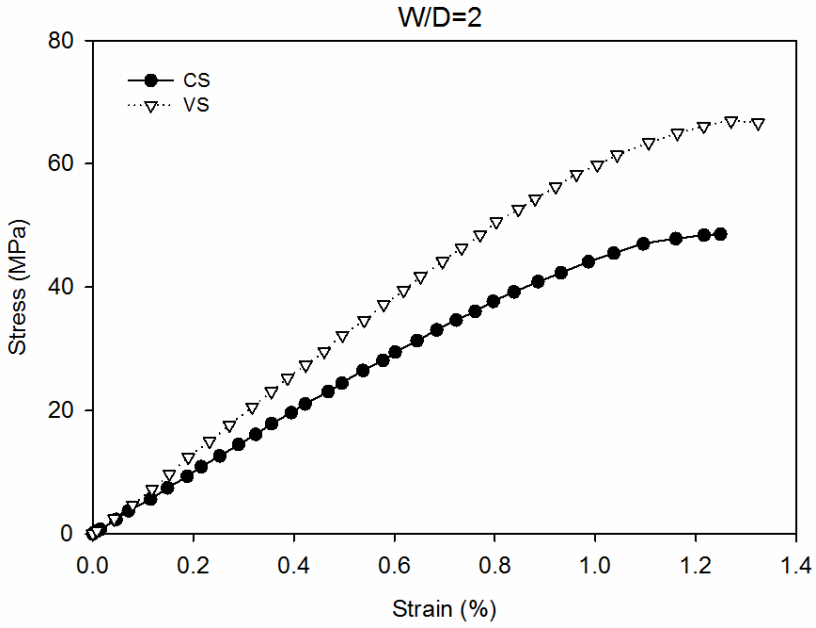

Figure 11. Stress-strain graph for CS and VS specimens with w/D=2.

It should be noted that extrudates are cut at the hole for the CS design, keeping only limited number of them around the hole. On the other hand, for the VS design, no extrudate is cut at the hole and they are all steered around the hole, filling the area around it. The difference in the materials distribution around the hole in the two cases can be clearly seen in the failed cross section imaging for CS and VS designs (Figure 12).

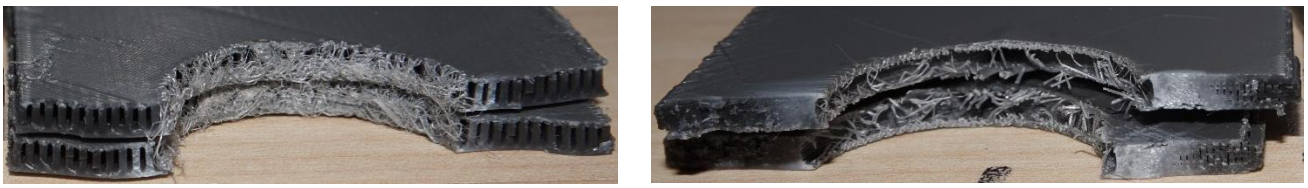

(a) **(b)**

Figure 12. The cross sections of failed specimens (w/D=2): (a) CS design; (b) VS design.

The stress-strain graph for a CS and a VS specimen with w/D=4 can be seen in Figure 13. Unlike the previous case (w/D=2), the improvement in failure strain is substantial with the use of CVS design, while improvement in failure stress is less pronounced.

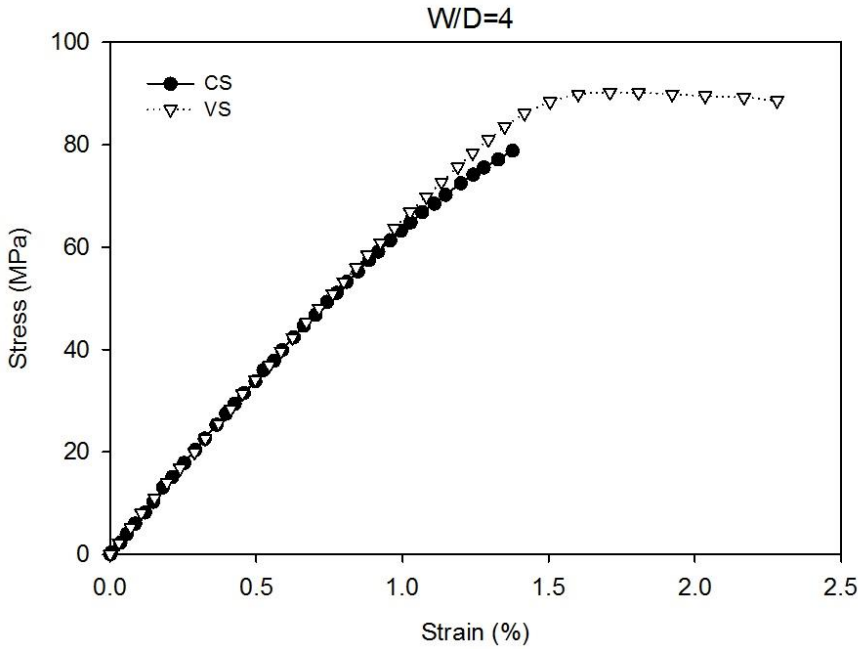

Figure 13. Stress-strain graph for CS and VS specimens with w/D=4.

As opposed to the straight rasters being cut at the hole (Figure 4b), the curvilinear ones are continuous (Figure 4a) and transfer the load smoothly around the hole. For w/D=2, the net section is small, thereby the ratio of the curvilinear rasters to the straight ones is a large value. As a result, the equivalent stiffness of the VS specimens is larger compared to that of the CS specimens. Conversely, for w/D=4, the ratio of the curvilinear rasters to the straight ones is much smaller and thus the equivalent stiffness of the VS and CS samples are close. For w/D=2, since the maximum stress at the hole is high, when the straight raster layers fail, the CVS layers also fail, resulting in a small improvement in failure strain. On the other hand, for w/D=4, since the maximum stress at the hole is small, when the straight rasters fail, the curvilinear ones still can carry the load before reaching their yield limit; thus, increasing the failure strain of the CVS specimens compared to the CS ones.

Table 3 summarizes ultimate strength and failure strain values obtained for open-hole tensile specimens with 2 configurations, w/D=2 and 4. For a large hole (w/D=2, D=18 mm) configuration, 38.0% improvement in the mean ultimate strength is obtained using VS design, while improvement in the mean failure strain is only 4.0%. For a small hole configuration (w/D=4, D=9 mm), improvement in tensile strength is 16.7%, while failure strain is increased by 52.5% compared with CS design. For both cases, Coefficient of Variation (CV) is below 5% for ultimate strength and it is below 10% for failure strain, which shows the reliability of the obtained results.

Table 3. Ultimate strength and failure strain for open-hole tensile specimens

Sample	Design	Ultimate Strength		Failure Strain	
		Mean (MPa)	CV	Mean (mm/mm)	CV
w/D=2	CS	48.0	1.84%	0.0125	8.97%
	VS	66.2	3.96%	0.0130	9.86%
w/D=4	CS	76.0	3.51%	0.0141	6.83%
	VS	88.6	4.53%	0.0215	6.53%

Open-hole tensile strength of CS and VS design for the two configurations (w/D=2 and 4) can be compared in Figure 14. Ultimate strength is calculated based on the gross cross-sectional area and the presence of the hole is disregarded. As a result, it is expected that the mean strength value increases by a reduction in the hole diameter (an increase in w/D parameter). It is also evident that for a larger hole diameter (w/D=2), higher improvement in mean strength is achieved using VS design compared with CS design. This signifies the importance of CVS 3D printing, especially for high stress concentration design cases, that enables manufacturing lighter and cheaper products.

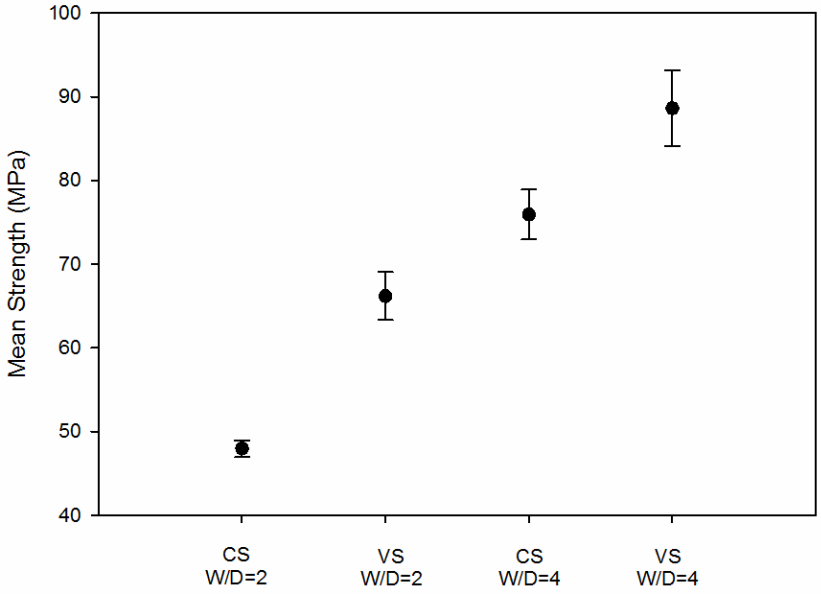

Figure 14. Mean strength for CS and VS designs for the two configurations (w/D=2 and 4).

4. Conclusion

Curvilinear Variable Stiffness (CVS) 3D printing has been explored to investigate potential improvements in open-hole tensile strength and failure strain of the specimens per ASTM D5766. An analytical approach has been described to find optimum curvilinear load paths using the analogy of field equations around a cylinder. For two hole diameters, Variable Stiffness (VS) and Constant Stiffness (CS) specimens have been designed and later manufactured using a commercial 3D printer. The Stress-strain graphs until failure have been created for the specimens, and ultimate strength and failure strain values have been calculated. We have observed that for the specimens with a larger hole diameter significant improvement in the ultimate strength is achieved, while the improvement in the failure strain is limited. On the other hand, for specimens with a smaller hole diameter, substantial improvement in failure strain is achieved, while the ultimate tensile strength improvement is less pronounced.

Future work is required to quantify the relationship between open hole tensile strength, and the terminated tool paths for CS and CVS paths as they vary as a function of the w/D. This can be used to develop an expression for the optimized selection between the two strategies and will require further mechanical testing of different w/D values. The results presented in this paper showed that 3D printing flexibility in manufacturing and anisotropic properties introduced by FFF can be utilized to improve structural performance of final parts. The approach of this study can be repeated with the use of highly directional materials as filaments in 3D printing, e.g. continuous carbon fibers. As a result, improvement in mechanical properties can be further increased and structural products for various applications across industries can be manufactured.

Acknowledgements

The authors would like to acknowledge the financial support provided by the Natural Sciences and Engineering Research Council of Canada (NSERC). We also would like to acknowledge Dr. Goetz Bramesfeld, Dr. Hamid Ghaemi and Jordan Kalman for their consultation and technical support.

References

1. Ning, F., et al., *Additive manufacturing of carbon fiber reinforced thermoplastic composites using fused deposition modeling.* Composites Part B: Engineering, 2015. **80**: p. 369-378.

2. Tekinalp, H.L., et al., *Highly oriented carbon fiber–polymer composites via additive manufacturing.* Composites Science and Technology, 2014. **105**: p. 144-150.

3. Mahajan, C. and D. Cormier. *3D printing of carbon fiber composites with preferentially aligned fibers*. in *IIE Annual Conference. Proceedings*. 2015. Institute of Industrial and Systems Engineers (IISE).

4. Ning, F., et al., *Additive manufacturing of carbon fiber-reinforced plastic composites using fused deposition modeling: Effects of process parameters on tensile properties.* Journal of Composite Materials, 2016. **51**(4): p. 451-462.

5. Türk, D.-A., C. Klahn, and M. Meboldt. *Combining additive manufacturing with CFRP Composites: design potentials*. in *Proceedings of the 20 th International Conference on Engineering Design ICED*. 2015.

6. Brooks, H. and S. Molony, *Design and evaluation of additively manufactured parts with three dimensional continuous fibre reinforcement.* Materials & Design, 2016. **90**: p. 276-283.

7. Dickson, A.N., et al., *Fabrication of continuous carbon, glass and Kevlar fibre reinforced polymer composites using additive manufacturing.* Additive Manufacturing, 2017. **16**: p. 146-152.

8. Carneiro, O.S., A.F. Silva, and R. Gomes, *Fused deposition modeling with polypropylene.* Materials & Design, 2015. **83**: p. 768-776.

9. Shojib Hossain, M., et al., *Improved Mechanical Properties of Fused Deposition Modeling-Manufactured Parts Through Build Parameter Modifications.* Journal of Manufacturing Science and Engineering, 2014. **136**(6).

10. Zaldivar, R.J., et al., *Influence of processing and orientation print effects on the mechanical and thermal behavior of 3D-Printed ULTEM ® 9085 Material.* Additive Manufacturing, 2017. **13**: p. 71-80.

11. Ziemian, S., M. Okwara, and C.W. Ziemian, *Tensile and fatigue behavior of layered acrylonitrile butadiene styrene.* Rapid Prototyping Journal, 2015. **21**(3): p. 270-278.

12. Lanzotti, A., et al., *The impact of process parameters on mechanical properties of parts fabricated in PLA with an open-source 3-D printer.* Rapid Prototyping Journal, 2015. **21**(5): p. 604-617.

13. Hill, N. and M. Haghi, *Deposition direction-dependent failure criteria for fused deposition modeling polycarbonate.* Rapid Prototyping Journal, 2014. **20**(3): p. 221-227.

14. Yau, S.S. and T.W. Chou. *Strength of woven-fabric composites with drilled and molded holes*. in *ASTM STP972, American Society for Testing and Materials*. 1988. Philadelphia, USA.

15. Hyer, M. and R. Charette, *Use of curvilinear fiber format in composite structure design.* AIAA Journal, 1991. **29**: p. 1011-1015.

16. Hyer, M. and H. Lee, *The use of curvilinear fiber format to improve buckling resistance of composite plates with central circular holes.* Composite Structures, 1991. **18**(3): p. 239-261.

17. Huang, J. and R.T. Haftka, *Optimization of fiber orientations near a hole for increased load-carrying capacity of composite laminates.* Structural and Multidisciplinary Optimization, 2005. **30**(5): p. 335-341.

18. Banichuk, N.V., *Optimization of Anisotropic Properties of Elastic Bodies*, in *Problems and Methods of Optimal Structural Design*, E. Haug, Editor. 1983, Springer US. p. 181-207.

19. Banichuk, N.V., V.V. Saurin, and A.A. Barsuk, *Optimal orientation of orthotropic materials for plates designed against buckling.* Structural optimization, 1995. **10**(3-4): p. 191-196.

20. Pedersen, P., *On thickness and orientational design with orthotropic materials.* Structural optimization, 1991. **3**(2): p. 69-78.

21. Pedersen, P., *Optimal Orientation of Anisotropic Materials. Optimal distribution of Anisotropic Materials. Optimal Shape Design with Anisotropic Materials. Optimal Design for a Class of Non-Linear Elasticity*, in *NATO ASI series E Applied Sciences.* 1993. p. 649-681.

22. Duvaut, G., et al., *Optimization of fiber reinforced composites.* Composite Structures, 2000. **48**(1–3): p. 83-89.

23. Tosh, M.W. and D.W. Kelly, *On the design, manufacture and testing of trajectorial fibre steering for carbon fibre composite laminates.* Composites Part A: Applied Science and Manufacturing, 2000. **31**(10): p. 1047-1060.

24. Li, R., et al. *Fiber steering around a cutout in a shear loaded panel*. in *47th International SAMPE Symposium and Exhibition*. 2002. Long Beach, CA, USA.

25. Li, R., D. Kelly, and A. Crosky, *Strength improvement by fibre steering around a pin loaded hole.* Composite Structures, 2002. **57**(1–4): p. 377-383.

26. Li, R., et al., *Improving the Efficiency of Fiber Steered Composite Joints using Load Path Trajectories.* Journal of Composite Materials, 2006. **40**(18): p. 1645-1658.

27. Tam, K.-M.M. and C.T. Mueller, *Additive Manufacturing Along Principal Stress Lines.* 3D Printing and Additive Manufacturing, 2017. **4**(2): p. 63-81.

28. Young, W.C. and R.G. Budynas, *Roark's formulas for stress and strain*. Vol. 7. 2002: McGraw-Hill New York.

29. Houghton, E., et al., *Aerodynamics for Engineering Students*. 2016: Butterworth-Heinemann.